JOURNAL OF THERMOPHYSICS AND HEAT TRANSFER
Vol. 20, No. 4, October–December 2006

Local Heat Transfer Measurements on a Curved Microsurface Using Liquid Crystal Thermography

R. Muwanga* and I. Hassan†
Concordia University, Montreal, Quebec H3G 2W1, Canada

DOI: 10.2514/1.17907

In this paper, local heat transfer measurements in circular mini- and microchannels are presented through the use of unencapsulated thermochromic liquid crystals for local wall temperature measurement. Microchannel heat transfer is fundamental to the design of a number of novel technologies in development for thermal control. Measurements are carried out in three different stainless steel tubes with nominal inner diameters of 1.07, 0.51, and 0.25 mm. The working fluids are distilled water and FC-72. A unique localized calibration of the thermochromic liquid crystal material is employed to minimize the effects of lighting nonuniformity and the effect of variable coating thickness. Local heat transfer and frictional pressure drop measurements are presented for the laminar, transitional, and turbulent flow regimes. The results are compared with correlations for both macro- and microchannels in the turbulent regime and show that, considering experimental uncertainty, both correlations are adequate for the experimental range investigated. Overall, the methods developed in this work demonstrate that the unencapsulated forms of thermochromic liquid crystals are a viable approach for temperature measurement in microheat transfer experiments.

Nomenclature

A	=	area, m^2
C_p	=	specific heat, $kJ/(kg \cdot °C)$
D	=	inner tube diameter, m
f	=	friction factor
h	=	heat transfer coefficient, $W/(m^2 \cdot °C)$
i	=	index
j	=	order of curve fit
k	=	thermal conductivity, $W/(m^2 \cdot °C)$
L_h	=	heated length, m
$\dot{m}$	=	mass flow, kg/s
Nu	=	Nusselt number
n	=	number of data points
$\tilde{P}$	=	power generated in tube, W
Pr	=	Prandtl number
q	=	heat flux, W/m^2
$\dot{q}$	=	heat generated, W/m^3
Re	=	Reynolds number, with respect to tube inner diameter
T	=	temperature, °C
x^*	=	$x/RePrD$
μ	=	viscosity, $N \cdot s/m^2$
ρ	=	density, kg/m^3
σ	=	surface tension, N/m

Subscripts

b	=	fluid bulk condition
fit	=	curve-fitted parameter
Fluid	=	fluid condition
i	=	inner wall
in	=	inlet condition
loc	=	local condition
o	=	outer wall
out	=	outlet condition
sat	=	saturation conditions
TLC	=	thermochromic liquid crystal
w	=	wall
x	=	streamwise location
∞	=	freestream condition

Received 27 May 2005; revision received 12 September 2005; accepted for publication 13 September 2005.

*Ph.D. Candidate, Department of Mechanical and Industrial Engineering.
†Associate Professor, Department of Mechanical and Industrial Engineering; ibrahimH@alcor.concordia.ca.

Introduction

IN recent years, the advent of very large integrated circuit technology (VLSI) has propelled the electronics industry into the fabrication of electronic circuits with feature sizes on the order of microns and submicrons [1]. This has allowed designers to pack these components with more features at much smaller tolerances and, in so doing, to improve the speed and performance of these electronics. However, as a result, there has been an increase in the heat produced per unit area, which, in turn, has generated the requirement for effective, miniaturized cooling technologies. One such device is the microchannel heat sink, which was pioneered in the early 1980s by Tuckerman and Pease [2]. These heat sinks demonstrated heat transfer rates about two orders of magnitude greater than those of commercial technologies for cooling arrays of integrated circuits [3]. The microheat sink/exchanger is characterized by a set of microchannels conventionally machined or micromachined into a conducting block.

A number of studies have been conducted in recent years in order to understand and improve the heat transfer performance of these devices with respect to microchannels [3–5]. Regarding single-phase heat transfer in mini- and microchannels, some recent reviews may be found in the literature [6–8]. Some of the prevalent characteristics and remarks related to single-phase continuum flows follows. There are discrepancies reported between mini- and microchannel results and the accepted correlations and trends for their macro counterparts. For example, the critical Reynolds number for transition to turbulent flow in mini- and microchannels has been reported to be as low as 200[8] compared with the commonly known approximate value of 2300. In addition, significant variations between the results of different investigators have been reported for the heat transfer coefficients and friction factors with no clear relationship in the differences in some instances [4]. Finally, the channel size at which deviations will occur from conventionally sized channels remains undetermined. With the exception of the confinement number for boiling flows, no physics-based classification of channel sizes has been proposed [9]. Overall, a review of the literature indicates the

need for additional and improved studies of heat transfer in mini- and microchannels [8].

Most work regarding experimental heat transfer measurements in mini- and microchannels use thermocouples (point sensors) for wall temperature measurements. One problem with such sensors is their large size compared with the channel dimensions and, hence, their potential influences on the flow characteristics. This may be alleviated by placing the sensors at a distance from the fluid-wall interface and assuming one-dimensional heat transfer or by using a fin analysis method [1]. These approximations, however, introduce inaccuracies in the internal wall surface temperature measurement. Also, the relative size of these sensors, if discreetly placed at the wall, gives only an area averaged temperature measurement. Another inconvenience of such point sensors is the need for an array of sensors to obtain full surface temperature measurements.

Nonintrusive techniques such as infrared (IR) thermography, laser-induced fluorescence (LIF), and liquid crystal measurements have traditionally been employed [10]. There are a variety of challenges associated with IR thermography, which include accurately characterizing its performance and calibration, determining the measured body's surface emmisivity, identifying the measurement point, and accounting for radiation losses and additional optical equipment [11]. In addition, for the measurement of micro-objects, accurately accounting for the background radiation is necessary. Hetsroni et al. [11], while measuring the surface temperature of a capillary tube of 1.5 mm outer diameter, used a technique whereby the background temperature was controlled to within that of the tube wall temperature. The aim of this was to minimize the uncertainty in measurement due to background radiation during IR measurement.

Thermochromic liquid crystal (TLC) thermometry is a nonintrusive technique based on the changing pitch size of the helical molecular structure of the material during temperature change. When illuminated with white light, TLCs will reflect light of a wavelength proportional to the temperature they are experiencing, and this reflected wavelength is proportional to the instantaneous pitch between molecular layers. Additional information about the characteristics of liquid crystals and their use in thermometry and heat transfer may be found in Ireland and Jones [12] and Hallcrest [13].

The TLC technique has been used by many researchers because the late 1960s when it was first applied to nondestructive testing (NDT) and flow visualization [14]. The successful use of TLCs on a microgeometry for thermal measurements has been demonstrated by Höhmann and Stephan [15] while investigating evaporation from a liquid meniscus. In their work, they used the unencapsulated form of TLCs applied to the backside of a 20-μm stainless steel foil. They were able to obtain spatial resolutions of 0.83 μm, where the uncertainty in temperature was 0.51°C or 7.5%. The use and limitation of the TLC method in boiling heat transfer has been investigated and has been discussed by Kenning et al. [16] and Klausner et al. [17]. These studies determined that, in many instances, due to the thermal lag between the liquid crystal and the inner wall surface, the response time of the liquid crystal is not sufficient to capture all the unsteady phenomena occurring during nucleation boiling.

A first glimpse at the use of TLCs in minichannels with boiling has been recently presented by Chin [18] and Chin et al. [19] during an investigation of boiling incipience and convective heat transfer in narrow vertical channels. These authors used the TLCs in their common microencapsulated (as opposed to unencapsulated) form, which, due to capsule diameters of 10–25 μm, restricts the spatial resolution capability of the TLC material. The use of unencapsulated TLCs for quantitative, high-resolution heat transfer measurements in small channels has, to a limited extent, been investigated [20]. This is likely due to the difficultly in handling unencapsulated TLCs, because they are easily contaminated by solvents or dust, and prolonged exposure to ultraviolet (UV) light can disturb their calibration and even destroy their response [13].

In the work of Aligoodarz et al. [20], rectangular channel geometries 2×1 mm and 2×2 mm with three walls made of 75-μm-thick stainless steel were studied for boiling flows. The fourth wall was made of glass, which was used for visualization, and the opposing stainless steel wall was coated with unencapsulated TLC. The authors document difficulties in obtaining a continuous coating of the TLC on the surface, as well as difficulties in accounting for its stringent requirements for a contaminant-free area. Their choice of the unencapsulated form, however, was motivated by the ability to apply it in thinner layers than the microencapsulated form, hence obtaining an improved response time, which was approximately 4 ms. Another benefit of the unencapsulated form is that the spatial resolution is now restricted to the optical configuration [21] and thus submicron resolution is possible. Unencapsulated TLCs were selected in the present work due to their potential for high resolution in comparison with infrared thermography, as well as due to the reduced hardware requirements in comparison to LIF. This paper describes the development of a local heat transfer measurement system for use on a curved microsurface using unencapsulated thermochromic liquid crystals.

Experimental Facility and Methodology

Flow Loop

A schematic of the main components employed in the closed-loop test facility are shown in Fig. 1. The flow loop concept was designed to accommodate boiling experiments that will be presented in a later study. Note that only the components relevant to the single-phase experiments are discussed here. The fluids used are distilled water and FC-72, a perfluorocarbon provided by 3M. The latter fluid was selected for its lower boiling point to accommodate boiling experiments in future work. Some relevant properties of FC-72 at room temperature are listed in Table 1.

Flow enters the loop from the main tank and is continuously circulated by a magnetically coupled gear pump (Fig. 1). The pump runs at a constant speed and supplies a flow rate of 290 ml/ min with a maximum pressure of 517 kPa (75 psi). A nutating digital output flowmeter provided by DEA Engineering is used to monitor the flow rate. This meter outputs a 5 V square wave signal at a frequency proportional to the time for the nutator to complete one cycle. The flowmeter was initially calibrated using the weighing method and has a reliable range from 10 ml/ min to 250 ml/ min. For very low flow rates, measurement was via tracking a fixed fluid volume over time. Upstream of the flowmeter is a 25-μm filter, which is used to remove any accumulating particles. A preheater is located at the test section for additional flow temperature control, whereas the exit of the test section has a cooler, which is used to restore the temperature of the fluid.

Test Channels

The test modules used are circular stainless steel tubing of nominal inner diameters 1.067 mm (0.042 in.), 0.512 mm (0.020 in.), and 0.254 mm (0.010 in.). Their corresponding hydraulic lengths were 152, 152, and 55 mm. The heated lengths were 105, 105, and 19 mm, respectively. This corresponds to hydrodynamic developmental lengths of 23.5 and 18 mm. The recent use of circular steel tubes in heat transfer studies of mini- and microchannels is by Lelea et al. [22] and Owhaib and Palm [23], using thermocouples, and Hetsroni et al. [11] and Hapke et al. [24], using infrared measurement. This study is the first, to the authors' knowledge, to provide single-phase heat transfer measurements using a thermographic technique for submillimeter-diameter tubes.

A half-section schematic of the circular tube test module used is shown in Fig. 2. A polycarbonate sheet was machined to produce the measurement chambers for pressure and temperature. The tubes are connected to these chambers using standard 0.0625-mm (1/16-in.) stainless steel compression fittings with specialty ferrules to accommodate the small-diameter tubing. The ferrule material is a composite of graphite and polymide, which has a high electrical resistance. The advantages of the compression fittings are that they are resealable and can withstand high pressures (~690 kPa rating). Copper stranded wire (14 AWG), was soldered to the tube to provide

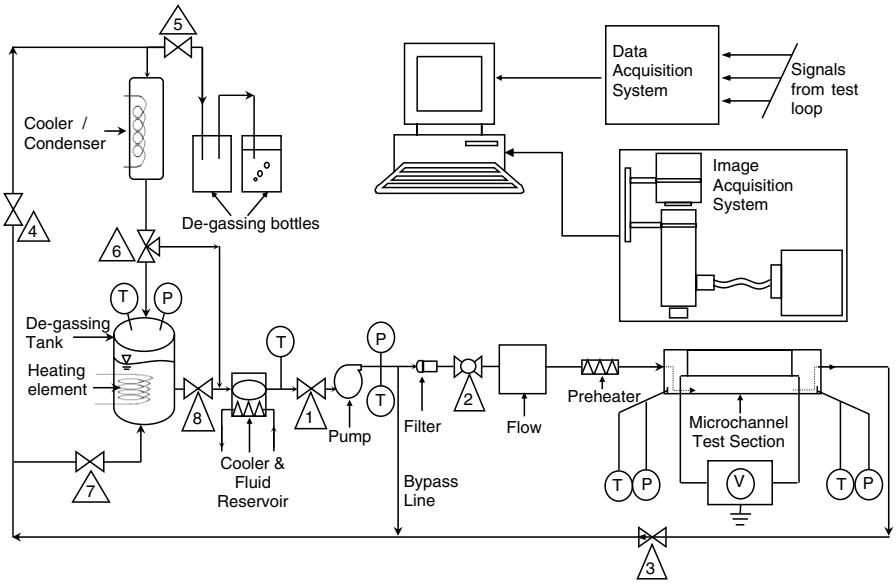

Fig. 1 Schematic of the experimental test facility.

the electrical lead connection. It should be noted that the present setup did not use any cover directly in contact with the TLC surface, due to the small size of the tube. Attempts were made to use optically transparent epoxies to encapsulate the tube, however, none of the ones tested were compatible with the TLC material. Rather a noncontacting cover was placed over the tube to protect the TLC-coated surface from dust and the room lights. The cover was an opaque plastic half tube that is open at both ends.

Unencapsulated Thermochromic Liquid Crystal Application

The aim of the TLC application procedure is to prepare a uniform coating that will produce vibrant colors. A thicker coating will improve the vibrancy, whereas too thick of a coating may start to produce nonnegligible temperature gradients through the TLC layer. Additionally, a variably thick layer will introduce uncertainty into the observed temperature field. A uniform coating has traditionally been applied through the use of an airbrush for the micro-encapsulated TLCs [12]. Application of the unencapsulated TLCs as documented by Höhman and Stephan [15], Aligoodarz et al. [20] and Kenning et al. [16] has been through use of a paint brush. However, Aligoodarz et al. mentioned significant difficulties in obtaining a continuous layer through this application methodology. According to Hallcrest [13], the liquid crystals (LCs) may be applied in their unencapsulated form through the dilution with an appropriate solvent, such as acetone, after which they are sprayed through an airbrush, resulting in an improved thin uniform layer. This approach, however, is usually not recommended, due to the hazardous nature of most solvents. Similar methodologies of applying unencapsulated LCs with an airbrush have been used for obtaining shear stress measurements, however. In these cases, the researchers diluted the LCs with petroleum ether [25] or with Freon [26] before applying them with an airbrush. No documentation, however, to the authors' knowledge, is available for the application of TLCs in their unencapsulated form via an airbrush.

Through trial runs of applying the TLCs with a paint brush, the difficulties observed by Aligoodarz et al. [20] were confirmed and, therefore, this methodology was considered inadequate for producing reliable results. The use of an airbrush was then selected and a variety of trials both of mixture concentration and of application were then performed to produce a sound application methodology. The solvent used was acetone and concentrations by weight of 20:1 (solvent to TLC) based on the suggestions of Hallcrest [13] were incorporated. Before coating, the tubes were cleaned with acetone. It was necessary to apply the coating under a fume hood, due to the toxic nature of the solvent used. This approach produced highly improved results in terms of coating uniformity and control of the coating. Specifically, unlike the paint brush coatings, no coating discontinuities were present and, at the working magnification, variations in the coating thickness were not visible. A Badger model 100 independent-action airbrush was used for application and it allowed for variation of the air to paint concentrations independently during spraying. To improve the color vibrancy of the TLC response, it is common to apply a coat of black paint before the TLC layer. This was incorporated in the current coating application using a water-based black paint and was also applied through the airbrush. The black paint layer is also advantageous, as it provides a protective layer against any residual contaminants that may be present on the metallic surface.

Table 1 FC-72 properties at 25°C and 1 atm[32]

ρ	1680 kg/m^3
μ	0.00064 N · s/m^2
σ	0.01 N/m
C_p	1100 J/kg · °C
Pr	12.35
T_{sat}	56°C

Measurement Apparatus

Two 1.5-mm-diam Type-T (Omega special error limits material) thermocouples were placed in each plenum chamber to measure the bulk fluid temperature (Fig. 2). A pressure transducer with a range of 0–517 kPa measured the pressure at the inlet plenum and a differential pressure transducer also with a range of 0–517 kPa

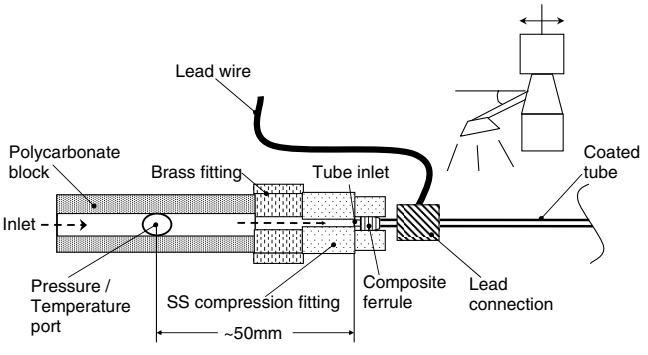

Fig. 2 Test module, symmetric half-section.

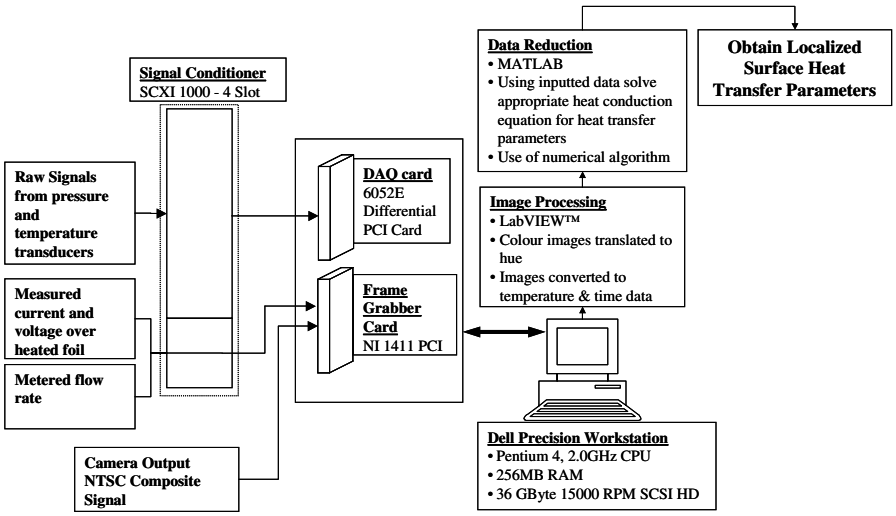

Fig. 3 Schematic of the data acquisition system.

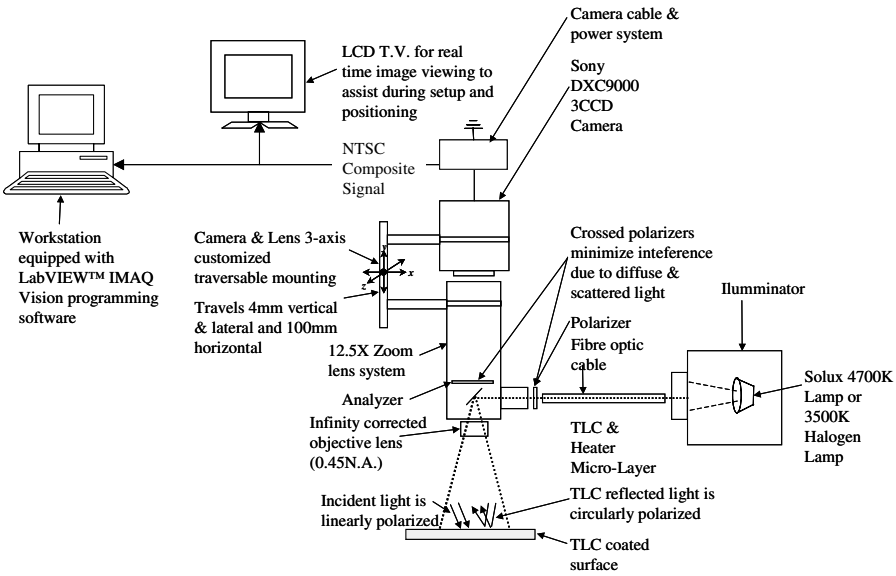

Fig. 4 Schematic of the image acquisition system.

measured the pressure difference between the two plenums. The output from these and other sensors was monitored through an automated data acquisition system using the LabVIEW^{TM} software. The data acquisition hardware consisted of National Instrument's SCXI 1000 signal conditioning unit with the appropriate modules and the NI 6052E 16-bit, 333 kHz data acquisition card. A schematic of the data acquisition system is shown in Fig. 3. Signals from the transducers were transferred through the signal conditioning unit, then to the computer, whereas the signals from the metering devices were directly transferred through the data acquisition card to the computer. Image acquisition was performed in LabVIEW and the images were captured at 640×480 pixel sizes in red-green-blue (RGB) format. The hue planes were simultaneously extracted and saved in tagged image file format (TIFF). Postprocessing of the images and acquired data was performed in MATLAB.

A detailed view of the image acquisition apparatus is shown in Fig. 4. Light originating from the illuminator box is directed through a single fiber optic cable. This has the advantage of keeping any heat generated by the light source away from the TLC-coated surface. An EKE-configured lamp was used with a color temperature rating of 3250 K. Light passes through a polarizer just before entering the zoom lens casing. Within the casing, it is deflected to the test surface by a beam splitter. Depending on the magnification required, the light may pass through an infinity-corrected objective for high-resolution measurements or else through the default auxiliary lens. Upon reflection from the surface, the light is circularly polarized. It passes into the zoom lens through the analyzer and is directed to the CCD camera. The crossed polarizing lens pair is available to obtain improved image quality. The light reflected by the TLC material is circularly polarized and thus travels through the crossed polarizing pair essentially unaffected. The acquired image is then transferred directly to the computer as a National Television System(s) Committee (NTSC) signal through a single BNC cable.

A liquid-crystal display (LCD) television was used for real-time monitoring and for positioning. The video signal used in the television loop comes from a separate output line in the camera, and the benefit of this is to minimize the accumulated noise that can occur by transferring the desired video signal through many components. Image acquisition is obtained using a Sony 3-CCD analog camera connected to a variable zoom microscopic video lens. The camera lens combination was mounted onto a three-axis traverse through variable-length stages, each with approximately a 1-μm resolution. This allowed for the length of the channel to be monitored through traversing the entire length. The lateral and vertical axis stages allow for fine-tuning of the position and focusing. Although the facility has the capability of a crossed polarizing illumination setup, this was not used for the circular tube configuration, due to the reduced intensity obtained when voltage was applied to the tube. The fiber optic illumination source was instead fixed onto the zoom lens at a fixed angle and directly illuminated the surface.

Heater power was obtained through two power supplies. One was a BK Precision switch mode power supply (model 1692) with a voltage range of 2.7–15 V and a maximum current rating of 40 A. The second was a Good Will (GW) Instruments power supply (model GPC-1850) with a voltage range of 0–5 V and a maximum current rating of 20 A. The unencapsulated liquid crystal material used was provided by LCR/Hallcrest. The TLC material nominally had a red start of 40°C with a bandwidth of 10°C.

Calibration Method

To obtain quantitative thermal data from the TLC response, a calibration of the material is required. The requirement of the calibration is to quantitatively relate the observed color to the material temperature. Different methods are available for quantifying the color observed; in the current work, the hue angle is taken as the color descriptor. The definition of hue H in the current work is the same as that recommended by Hay and Hollingsworth [27], which is

$$H = \arctan\left(\frac{\sqrt{3}(G-B)}{2R-G-B}\right) \tag{1}$$

The perceived color of a TLC will depend upon the primary and background light spectral characteristics, the camera viewing angle and distance, the primary lighting angle and distance, the lights optical path, and the instance of the TLC application. For a calibration to be fully valid, the preceding must be maintained between the calibration and the experiment. This is usually done through an in situ calibration [28]. Choices for calibration include a linear temperature gradient [29], a liquid bath or circulated liquid [27], or an isothermal block [28]. A linear temperature gradient applied to a metal block is advantageous in providing a quick calibration, however, the amount of calibration points is dependent on the number of sensors employed along the gradient. An isothermal bath or circulated bath provides the best means of obtaining a truly isothermal surface, however, it does require a liquid supply that is either stirred or circulated. A constant temperature block is usually difficult to work with in maintaining the full viewing surface isothermal and, hence, not recommended.

For the present study, a calibration based on circulating the fluid through the channel was selected, due to its ease of incorporation into the setup. The temperatures at the tube inlet and outlet were measured and remained within 0.5°C of each other. The fluid was slowly heated via the preheater and images captured at incremental changes in temperature. One of the main observations from this work is that the response of the unencapsulated TLC under increasing magnification will contain varying degrees of noise and scatter. Figure 5 shows the histogram of a color response from a constant temperature region 30×600 pixels. To address this in an automated fashion, an intelligent calibration process is introduced.

To start calibration, a region of interest (ROI) needs to be selected to base the calibration curve on. Lighting, viewing angle, and coating uniformity may all influence the calibration between two different regions on the tube. To eliminate such influences, a calibration curve was produced for a number of regions in the image. The minimum size for a given ROI is a single pixel; however, to account for noisy pixels using statistics, an ROI size greater than one pixel was used. Because the camera was traversed, this meant that the ROI would be a particular tube location and that high accuracy in traversing between set locations was pertinent. The ROI should not be too large, because local variabilities will not be captured. For the present work, an ROI of 4×3 pixels and 4×2 pixels was incorporated. A typical image size of 60×640 pixels with an ROI of 4×3 pixels gives 3200 calibration curves.

Two calibrations methods were used. In the first, the fluid was incrementally heated and, at each increment, images were captured at each of the locations. This method produced only a few calibration points for each location. To improve on this, our second approach consisted of heating incrementally at a fixed location and capturing

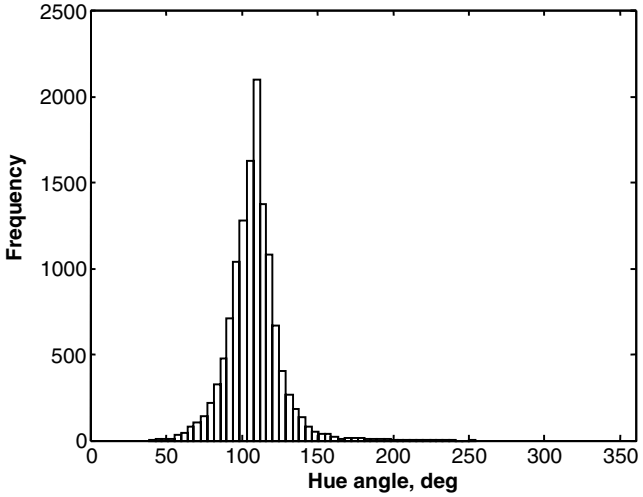

Fig. 5 Constant temperature region hue angle histogram.

the full bandwidth before moving to the next location. This method is implemented for all the measurements using FC-72 and is the finalized method of choice for all future work. The main issue is to minimize the calibration time and capture as many points as possible. In the first approach, calibration time was on the order of 3 h and few data points were captured. In the second approach, we were able to take advantage of the fluid's inevitably increasing temperature and, therefore, because the camera was at a fixed location, it would continuously capture images as the temperature slowly rose. The rate of heating was approximately 0.5°C/ min.

The aim of the curve fit is to produce a monotonically increasing relationship. Depending on the quality of the data points for each ROI, this was not always possible. Extraneous cases would have maxima or minima locations in the curves. To automatically determine a calibration data curve fit that did not contain extraneous regions, the following logic was implemented:

1) Sort the data set with respect to increasing hue.

2) Starting from the minimum hue value, only keep data points that have a positive change in temperature with respect to increasing hue.

3) Fit a fifth-order polynomial curve to the modified data set.

4) If any maxima or minima exist in the hue range of 25–175, discard the fifth-order polynomial curve and fit a third-order polynomial curve.

5) If any maxima or minima exist in the hue range of 25–225, modify the data set's zero location to a predefined temperature.

6) If any maxima or minima exist in the hue range of 100–175, abandon curve fitting and use the neighboring ROI instead.

The ranges were selected based on repeated observations of curve fits. The change of hue range between steps 4 and 5 was due to the change in characteristics of the two polynomial types applied to the same data set. The change of hue range between steps 5 and 6 was because once a third-order fit was applied and the zero location fixed, if an extremity in the curve occurred in the hue range of 25–100, it was a very slight minima that could be disregarded. That is, the temperature dip at the minima was less than 0.1°C.

The hue angle is defined on a polar system and, hence, due to scatter; hue values close to 0 deg may be present in the 300 to 360 deg range and vice versa for hue values close to 360 deg. Compensation similar to that of Hay and Hollingsworth [27] was incorporated, whereby the negative angle was used when such scatter occurs. This can be identified, for example, when at high temperatures a low hue value is obtained, or when at low temperatures, a high hue value is obtained. The ROI will have a particular scatter in the hue values, and, for the present study, the nominal hue value was based on the median of the hue values. Figure 6 shows a good fifth-order curve fit. The circles are the section of the data set that is kept after sorting. Figure 7 shows the modification of a fifth-order fit to a third-order fit, due to a maximum in the curve fit. Once again, the circles are the section of the data set that are kept after sorting.

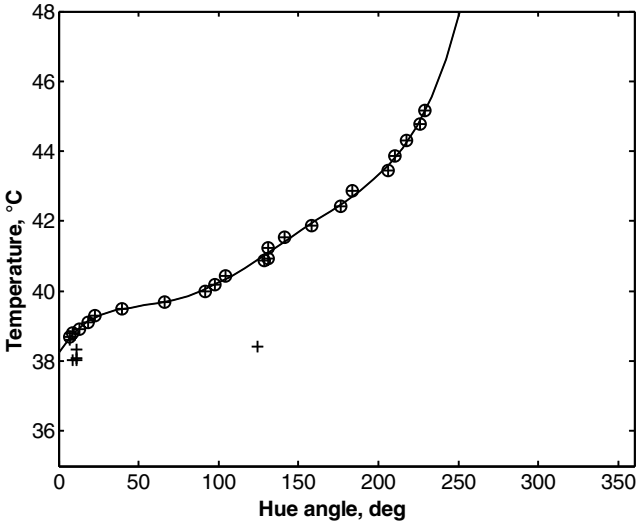

Fig. 6 Calibration fit; fifth-order typical good.

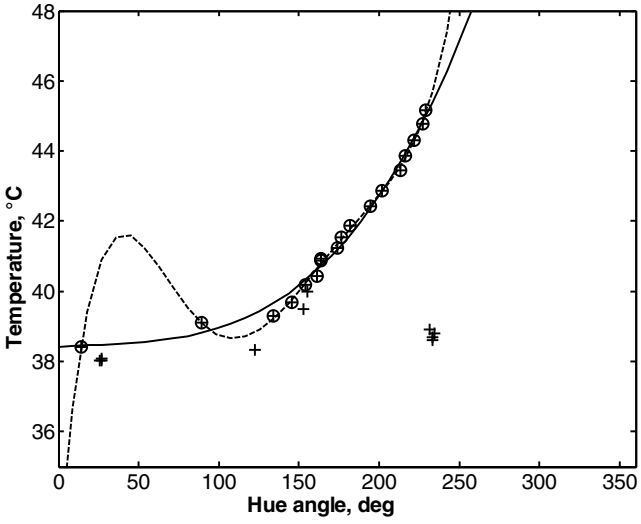

Fig. 7 Corrected calibration curve with fifth-order and third-order fits.

Test Procedure and Data Reduction

Procedure

Before each experiment, the TLC material was calibrated as described in the previous section. To begin measurements, the flow rate was set by adjusting the bypass valve and the system was then left to run for about ten minutes. The room lights were dimmed and the tube was kept covered. Traversing began at the rear of the tube, where the wall temperature would be highest. The configured magnification provided a field of view of 10.233×7.671 mm for the 1- and 0.5-mm tubes and a field of view of 6.697×5.020 mm for the 0.25-mm tube. This translates into 15.528 and 10.1626 μm/pixel. Although the facility's magnification capabilities are much larger, a higher magnification would have required more traversing in order to capture the entire tube. This would require more time and provide additional information unnecessary for the purpose of the present work. After running flow through the system, measurements were ready to be taken and the cover was removed. The illumination system was turned on and the voltage was slowly adjusted until the majority of the TLC color response was in the green/blue range. The system was then allowed to come to equilibrium, which spanned 5–10 minutes, and afterwards, a measurement was taken.

Three images were captured at a speed of 30 frames per second. These color images were converted to hue angle, scaled on an integer range from 0–255, and then averaged for each pixel location.

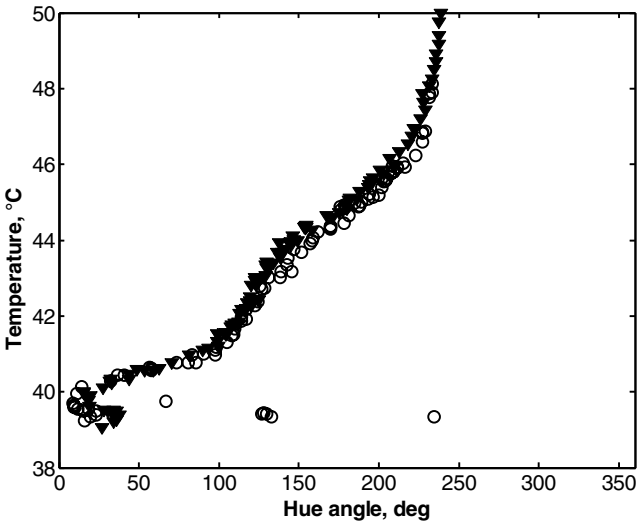

Fig. 8 Calibration curves accumulated over different time periods.

Simultaneously, the fluid temperature at inlet and outlet, as well as the flow rate measurements, were captured. For each traversed location, two to four measurements were captured at a given flow rate, though the heater power may be adjusted between image capture. During data reduction, the best images by visual inspection were selected for final data reduction. Whenever the voltage was adjusted, the illuminating system was turned off in order to minimize any degradation to the TLC and external heat addition to the tube as the system approached equilibrium.

The TLC calibration may change slightly over time. It was important, then, to verify that over a measurement run, which could be as long as three h, the calibration curve would not shift significantly. To verify this, calibration data at a fixed location were obtained at two different times, 3.5 h apart. Between this time period, the tube was left uncovered to simulate the experimental runs. Figure 8 shows the data obtained from these two calibration runs, determined from a ROI size of 4×3 pixels. As can be seen in Fig. 8, the change in the calibration curve is insignificant, with a maximum temperature change of approximately 0.5°C. Hence, the calibration taken before the measurements runs can be used over the entire measurement period. Once an experimental run was completed, the tube remained covered.

Data Reduction

The friction factor was obtained from the pressure drop relation:

$$\Delta P = \left(f \frac{L}{D} + K_{\text{loss}} \right) \frac{\rho V^2}{2} \tag{2}$$

The losses at the entrance and exit (K_{loss}) were estimated from Streeter [30], considering the area changes at each location between the pressure port and the tube entrance and exit.

The local Nusselt number was calculated as

$$Nu_x = \frac{h_x D}{k_{\text{loc}}} \tag{3}$$

The local heat transfer coefficient h_x was obtained through the convective heat transfer relation with the following parameter definitions:

$$h_x = \frac{q''}{(T_{w,xy} - T_{b,x})} \tag{4}$$

The heat flux to the fluid was calculated based on the power applied to the tube and corrected for losses to the environment. This is given by

$$q'' = \frac{\tilde{P}_{\text{tube}} - h_\infty A_{o,\text{heated}}(T_{w,\text{TLC}} - T_\infty)}{A_{i,\text{heated}}} \tag{5}$$

The external heat transfer coefficient was obtained from tests with no fluid circulating and a constant power applied to the tube. The power to the tube is the measured voltage and current, corrected for power loss across the lead connections. Comparisons were made between the fluid enthalpy rise based on measured inlet and outlet temperature differences vs the electrical power applied to the tube. These differences were found to be within 5% of each other for the majority of the cases. However, in a few cases where the fluid bulk temperature rise was low, differences were on the order of 20–40%; this can be attributed to fluid temperature measurement uncertainty.

The internal wall temperature was calculated assuming 1-D heat conduction through the wall, with the outer wall temperatures measured by the TLCs as boundary conditions. That is given by

$$\begin{gathered} \frac{1}{r}\frac{\partial}{\partial r}\left(r\frac{\partial T}{\partial r}\right) + \frac{\dot{q}}{k} = 0 \\ T(r_o) = T_{w,\text{TLC}} \\ -k\frac{\partial T(r_o)}{\partial r} = h_\infty(T_{w,\text{TLC}} - T_\infty) \end{gathered} \tag{6}$$

then the inner wall temperature $T_{w,i}$ is given by

$$\begin{aligned} T_{w,i} - T_\infty &= -\frac{r^2}{4}\frac{\dot{q}}{k} + C1 \cdot \ell_n(r) + C2 \\ C1 &= -\frac{r_o h_\infty}{k}(T_{w,\text{TLC}} - T_\infty) + \frac{r_o^2 \dot{q}}{2k} \\ C2 &= (T_{w,\text{TLC}} - T_\infty) + \frac{r_o^2}{4}\frac{\dot{q}}{k} - C1\,\ell_n(r_o) \end{aligned}$$

The differences between the inner and outer wall temperature were minor, however, and typically less than 0.3°C.

The local fluid bulk temperature $T_{b,x}$ was determined from an energy balance and at each streamwise location was

$$T_{b,x} = T_{\text{in}} + \frac{\pi D q''}{\dot{m} C p} \cdot x \tag{7}$$

Properties for the preceding calculations, except the local Nusselt number, were based on the average fluid temperature between inlet and outlet. The properties were obtained from Kays and Crawford [31] for water and 3M product information [32] for FC-72.

Uncertainty

The uncertainty in the TLC temperature was calculated similar to the methods discussed in Hay and Hollingsworth [27] and in Chin [18]. The wall temperature uncertainty was taken to be

$$\delta T_w = \sqrt{\left(\frac{\mathrm{d}T}{\mathrm{d}H}\delta H\right)^2 + \delta T_{\text{Fluid}}^2 + (2 \times \text{SEE})^2} \tag{8}$$

where

$$\frac{\mathrm{d}T}{\mathrm{d}H}$$

is the sensitivity in the temperature hue curve, which was either a fifth- or third-order polynomial, as discussed earlier. Also, δH represents the standard deviation in hue for the ROI, and, because the ROI was small (<12 pixels), a constant value of 1 deg was selected instead. In addition, δT_{Fluid} was the uncertainty of the thermocouple probes used to measure the fluid temperature during calibration. Finally, the standard error estimate (SEE) takes into account the error in the polynomial curve fit and is typically defined as

$$\text{SEE} = \left[\sum_{i=1}^{n}[T_i(h) - T_{\text{fit},i}(h)]^2/(n - j - 1)\right]^{1/2} \tag{9}$$

This value was less than 0.50°C for all cases and was higher for third-order fits vs fifth-order fits.

Typical uncertainties in wall temperature measurement were estimated to be ±1.02°C and are similar to that of other researchers [19]. Uncertainties in pressure drop measurement were ±3.6 kPa based on instrument specifications and ±0.7°C for fluid temperature measurement based on manufacturer specifications of the combined measurement system (thermocouple and signal conditioning unit). Diameter-dependent uncertainties included the tube inner and outer diameter and the flow rate and Nusselt number and are listed in Table 2. Note, the diameter uncertainties are based on manufacturing tolerance.

Table 2 Typical uncertainties for diameter-dependent parameters

Nominal tube diameter	Inner diameter	Outer diameter	Flow rate	Nusselt no.
0.254 mm	±0.0254 mm	±0.0127 mm	±0.5 ml/min	14–17%
	±0.0254 mm	±0.0127 mm	±1.5 ml/min	8–18%
0.508 mm	−0.0127 mm	−0.0000 mm		
1.067 mm	±0.0254 mm	±0.0127 mm	±1.5 ml/min	9–18%

Results

Figure 9a and 9b show a pair of data sets from raw image to processed data. Figure 9a is considered a good data set and is typical of the data presented. In the figures, the temperature is rising from left

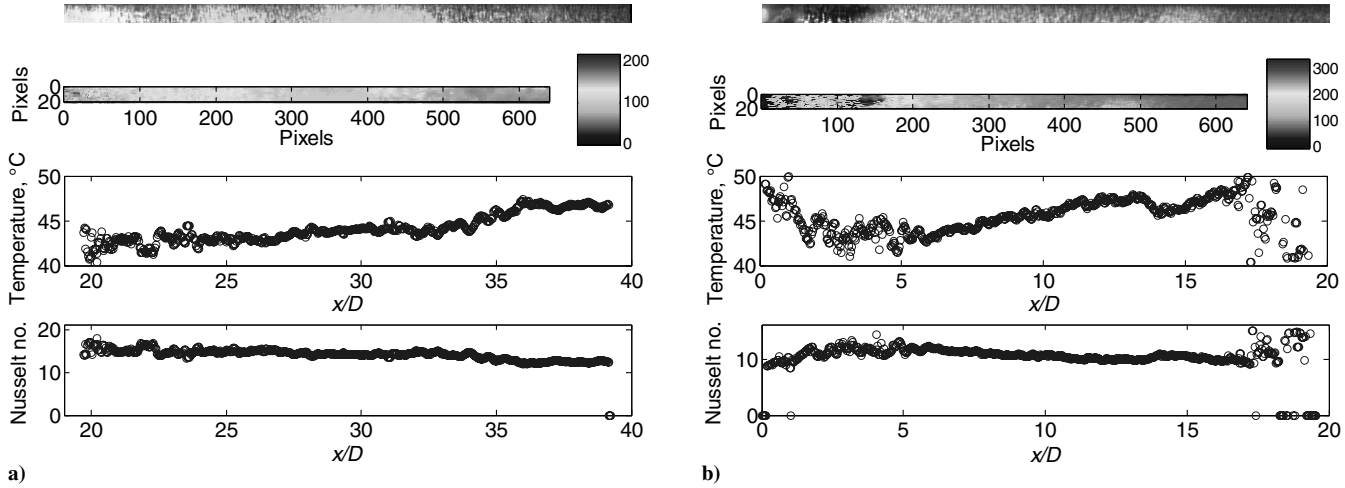

Fig. 9 Typical image data sets, raw data to processed data: a) good data set and b) bad data set.

to right and covers a distance of approximately 10 mm. In Fig. 9a, there is some minor scatter in the red range, due to the large light intensity, however, in the green/blue range, the response is much better. Most of the data presented is derived from images that fell in this green/blue range. Figure 9b only has a small useful region, therefore, such a data set is not considered in the final presentation.

Figures 10–14 show the circumferentially averaged streamwise Nusselt number. The data are compiled from a number of traversed locations and the heat flux used was not always constant. This is one of the main contributions of scatter observed. In spite of this, for the majority of the plots in the laminar regime (taken as $Re < 2300$), a decreasing Nusselt trend is observed with increasing distance, approaching an asymptotic value. Although for some laminar cases the downward slope is minimal, their slope tends to be more significant than for the turbulent and transitional cases. For the remaining cases, the Nusselt number is constant. The decreasing vs constant trend of laminar vs turbulent flows are as expected, based on physical considerations and observations in larger tubes [33]. For data in the turbulent regime, a short developmental length is observed, which can be generalized as being less than 10 hydraulic diameters. Shown in Figures 15–18 are the local heat transfer results for the laminar regime data. The results show that the developmental length for the laminar results are well represented by the analytical solution given in Shah and London [34]. In the fully developed region, the Nusselt number tends to the analytical result of 4.364, which is for constant heat flux in a circular tube. The results show no unexpected trend related to decreased tube diameter. The friction factor results are shown in Fig. 19. They are compared with the friction factor for fully developed laminar flow in a pipe, given by

$$f = \frac{64}{Re} \tag{10}$$

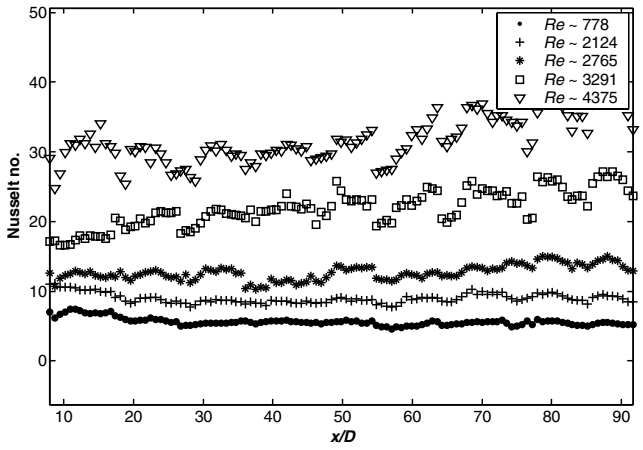

Fig. 10 Streamwise Nusselt number; 1.0 mm, H_2O.

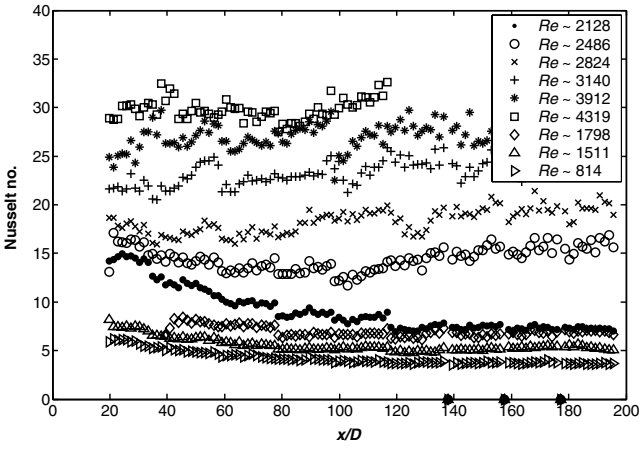

Fig. 11 Streamwise Nusselt number; 0.5 mm, H_2O.

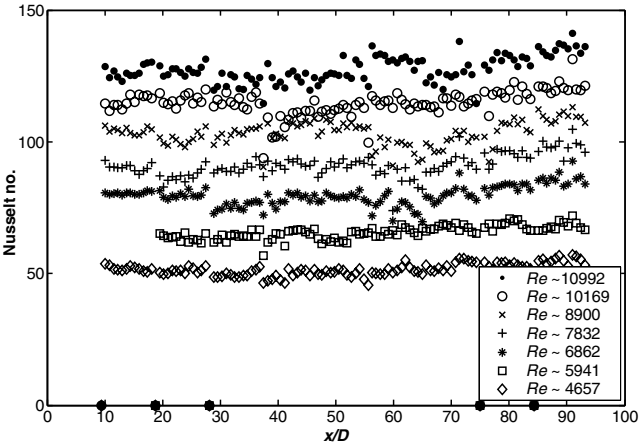

Fig. 12 Streamwise Nusselt number; 1.0 mm, FC-72.

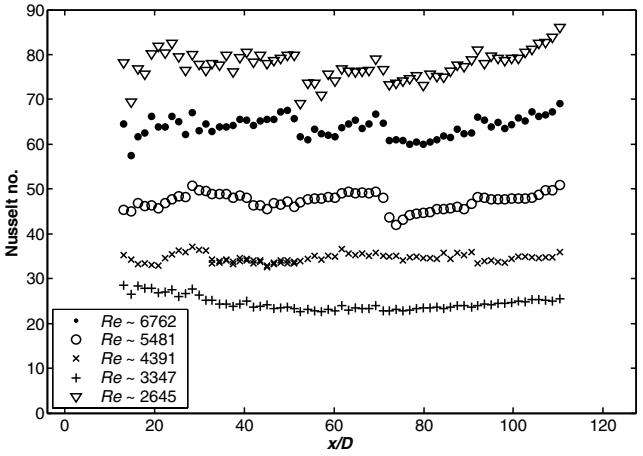

Fig. 13 Streamwise Nusselt number; 0.5 mm, FC-72.

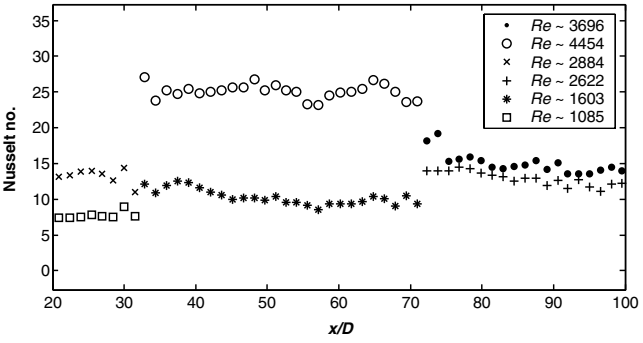

Fig. 14 Streamwise Nusselt number; 0.25 mm, FC-72.

[35] and

$$f = [1.82 \times \log(Re) - 1.64]^{-2} \tag{11}$$

[36] for fully developed turbulent flow. Equation (11) was selected due to its use in the average Nusselt number relation to be presented later. Very good agreement is observed for all diameters in the laminar range. In addition, the predicted curves show very good agreement for the 1-mm-diam tubes in the turbulent regime. For the 0.5-mm case, the results are underpredicted by Eq. (11). This equation, though, is valid for smooth tubes with a $Re > 10^4$. This may suggest an increasing tube roughness influence with decreasing diameter, however, as seen later for the average Nusselt number results, no benefit in heat transfer is gained from the higher friction factor. Rather, it suggests that the estimated entrance and exit loss factors are the cause of the differences observed.

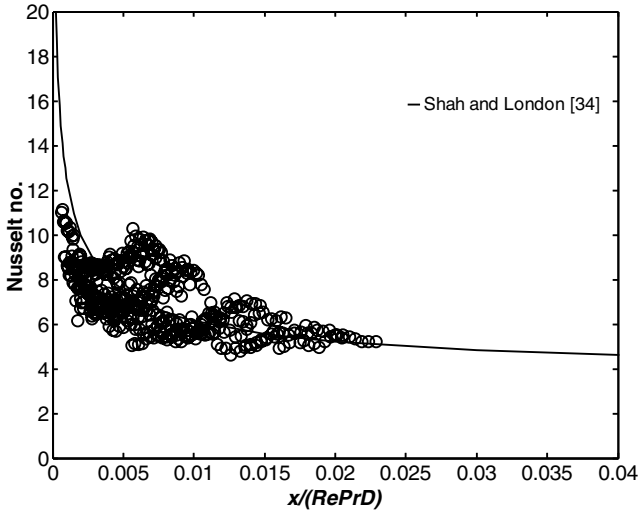

Fig. 15 Laminar streamwise Nusselt number; 1.0 mm, H_2O.

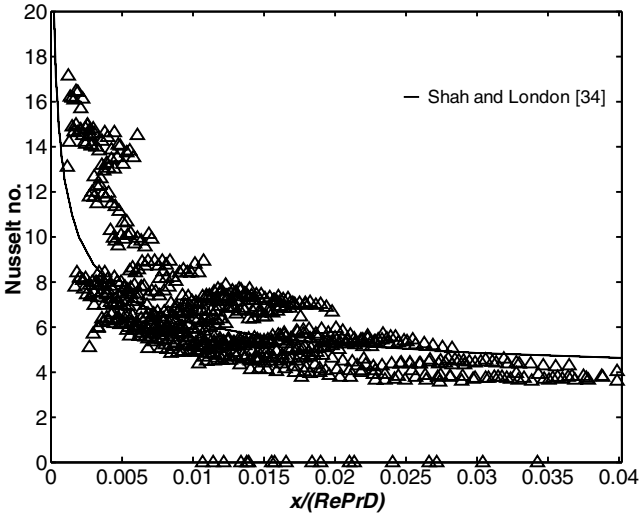

Fig. 16 Laminar streamwise Nusselt number; 0.5 mm, H_2O.

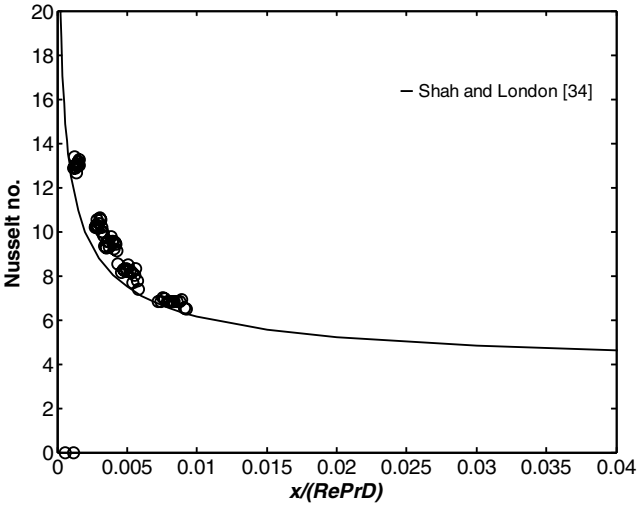

Fig. 17 Laminar streamwise Nusselt number; 1.0 mm, FC-72.

The transition for both the 1-mm and the 0.5-mm tubes is observed between a Reynolds number of 2000 and 4000. This is observed for both fluids and shows that the conventional value of 2300 is reasonable for these two diameters. For the 0.25-mm case, however, a delayed transition is observed and the curve appears to be changing direction at a Reynolds value of about 5000.

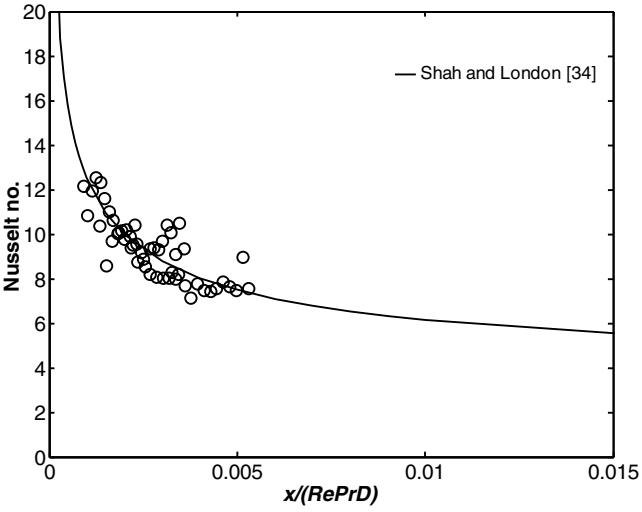

Fig. 18 Laminar streamwise Nusselt number; 0.25 mm, FC-72.

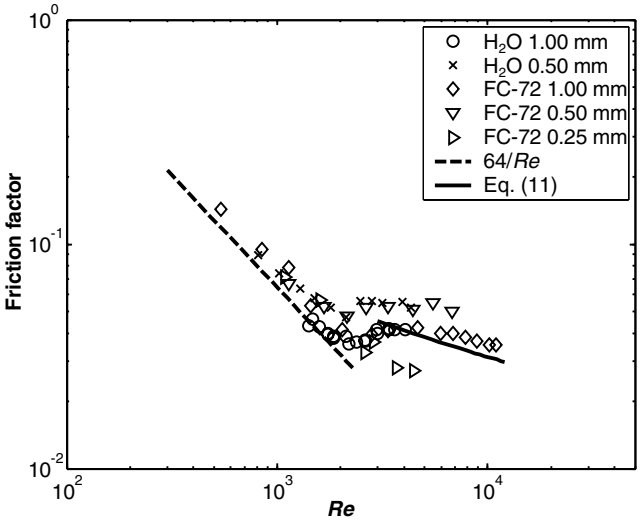

Fig. 19 Friction coefficient.

The average Nusselt number for all the tube diameters and the two fluids is shown in Fig. 20. These data are obtained from the average of the farthest downstream image captured, to allow for thermal development. The Nusselt number is divided by $Pr^{0.4}$ to account for the two differing fluids. The data are compared with two correlations, one the Gnielinski [36] correlation representing large tubes and given by

$$Nu_{\text{Gniel}} = \frac{(f/8)(Re - 1000)Pr}{1 + 12.7(f/8)^{1/2}(Pr^{2/3} - 1)} \tag{12}$$

Similar to Gnielinski [36], the friction factor is determined from Eq. (11). The second is a correlation given by Adams et al. [37] and representing small-diameter channels. It is based on the Eq. (12), with a slight modification as follows:

$$Nu_{\text{Adam}} = Nu_{\text{Gniel}}(1 + F) \tag{13}$$

where

$$F = 7.6 \times 10^{-5} Re[1 - (D/1.164)^2]$$

The data are well correlated between each other, particularly, between the 0.5-mm and 1.0-mm tubes at higher Reynolds. The

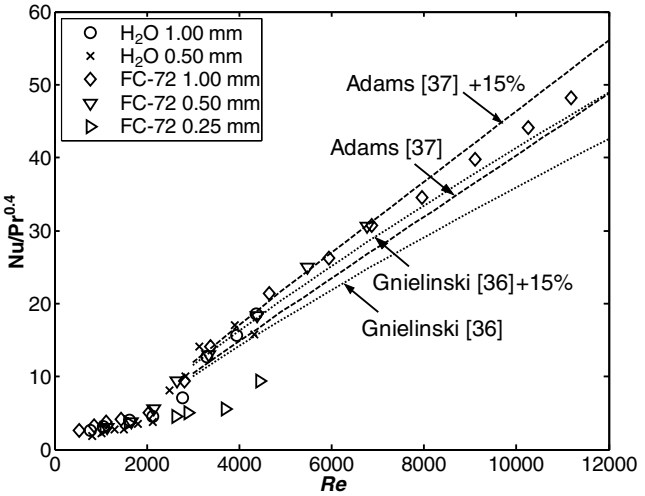

Fig. 20 Average Nusselt number.

influence of the delayed transition for the 0.25-mm FC-72 case is reflected also in the average Nusselt number (Fig. 19). Comparing the data with the correlations, at first glance, the Adams et al. [37] correlation appears to be the better choice. However, when considering the experimental uncertainty of the experiment, correlation, or both (taken as 15%), the Gnielinski [36] correlation also demonstrates an adequate comparison. Tube roughness is not considered a major influence, as both tubes showed differing friction factors yet similar Nusselt numbers. The conclusion, therefore, is that in the operational range considered of $Re < 10^4$ and Prandtl number 5.4–11.5, and with experimental uncertainties kept in mind, both the Gnielinski correlation for large tubes and the Adams correlation suggested for small tubes are adequate. Further, as a conservative design guideline, when determining the heat load applied, the Adams correlation should be used, whereas when estimating the cooling benefit gained, the Gnielinski correlation should be used. These guidelines are deemed general, as there will be few applications of tubes in the submillimeter range with Reynolds numbers exceeding 10^4, as the pressure drop becomes unrealistically large.

Conclusions

This paper presents two main contributions related to heat transfer in microgeometries. The first is the development of a method using unencapsulated thermochromic liquid crystals for local heat transfer measurements on curved microsurfaces, specifically, a circular tube. To the authors' best knowledge, this is the first use of this form of liquid crystals and of a thermographic technique for heat transfer measurements in submillimeter-sized tubes. A localized calibration is used to minimize the influence of lighting, viewing, and local variabilities. A large number of calibration curves are obtained from this approach and, thus, automation and logical filtering are implemented.

The second point, which has been enabled due to the first, is local single-phase heat transfer measurements in small-diameter tubes of nominal size (0.254, 0.512, and 1.067 mm) covering the laminar, transitional, and turbulent regimes.

The results demonstrate that the conventional size analytical solution for laminar flow is adequate for predicting the local heat transfer in thermally developing flows inside submillimeter-sized circular tubes of the range studied.

Local Nusselt numbers in the turbulent regime are shown to have a developmental length less than approximately $10x/D$, which is similar to conventionally sized tubes in this Prandtl number range. Considering uncertainties in Nusselt number correlations and the present data, both the conventional correlation given by Gnielinski [36] and the microchannel correlation given by Adams et al. [37] are adequate for predicting averaged Nusselt numbers in circular tube diameters ranging from 0.25–1 mm, for $2500 \leq Re \leq 10^4$ and Prandtl number 5.4–11.5. Finally, the choice of the correlation should be based on the amount of conservatism required in the design.

References

[1] Qu, W., and Mudawar, I., "Flow Boiling Heat Transfer in Two-Phase Micro-Channel Heat Sinks-I. Experimental Investigation and Assessment of Correlation Methods," *International Journal of Heat and Mass Transfer*, Vol. 46, No. 15, 2003, pp. 2755–2771.

[2] Tuckerman, D. B., and Pease, R. F. W., "High-Performance Heat Sinking for VLSI," *IEEE Electron Device Letters*, Vol. EDL-2, No. 5, 1981, pp. 126–129.

[3] Zohar, Y., "Microchannel Heat Sinks," *The MEMS Handbook*, edited by M. Gad-el-Hak, McGraw–Hill, New York, 1998, pp. 32-1–32-30.

[4] Mehendale, S. S., Jacobi, A. M., and Shah, R. K., "Fluid Flow and Heat Transfer in Micro- and Meso-Scales with Application to Heat Exchanger Design," *Applied Mechanics Reviews*, Vol. 53, No. 7, 2000, pp. 175–193.

[5] Hassan, I., Phutthavong, P., and Abdelgawad, M., "Microchannel Heat Sinks: An Overview of the State-of-the-Art," *Microscale Thermophysical Engineering*, Vol. 8, No. 3, 2004, pp. 183–205.

[6] Morini, G. I., "Single-Phase Convective Heat Transfer in Microchannels: A Review of Experimental Results," *International Journal of Thermal Sciences*, Vol. 43, No. 7, 2004, pp. 631–651.

[7] Bailey, D. K., Ameel, T. A., Warrington, R. O., and Savoie, T. I., "Single Phase Forced Convection Heat Transfer in Microgeometries: A Review," *Proceedings of the Intersociety Energy Conversion Engineering Conference (IECEC)*, American Society of Mechanical Engineers, New York, 1995, pp. 141–147.

[8] Sobhan, C. B., and Garimella, S. V., "A Comparative Analysis of Studies On Heat Transfer and Fluid Flow in Microchannels," *Heat Transfer and Transport Phenomena in Microscale*, Begell House, New York, 2000, pp. 80–92.

[9] Thome, J. R., "Boiling in Microchannels: A Review of Experiment and Theory," *International Journal of Heat and Fluid Flow*, Vol. 25, No. 2, 2004, pp. 128–139.

[10] Goldstein, R. J., Chen, P. H., and Chiang, H. D., "Measurement of Temperature and Heat Transfer.," *Handbook of Heat Transfer*, 3rd ed., McGraw–Hill, New York, 1998, pp. 16.1–16.77.

[11] Hestroni, G., Mosyak, A., Segal, Z., and Ziskind, G., "A Uniform Temperature Heat Sink for Cooling of Electronic Devices," *International Journal of Heat and Mass Transfer*, Vol. 45, No. 16, 2002, pp. 3275–3286.

[12] Ireland, P. T., and Jones, T. V., "Liquid Crystal Measurements of Heat Transfer and Surface Shear Stress," *Measurement Science and Technology*, Vol. 11, No. 7, 2000, pp. 969–986.

[13] Anon., "Hallcrest Product Information," Hallcrest, Repts. DS-001–DS-010, Glenview, IL, 2000.

[14] Fergason, J. L., "Liquid Crystals in Nondestructive Testing," *Applied Optics*, Vol. 7, No. 9, Sept. 1968, pp. 1729–1737.

[15] Höhmann, C., and Stephan, P., "Microscale Temperature Measurement at an Evaporating Liquid Meniscus," *Experimental Thermal and Fluid Science*, Vol. 26, June 2002, pp. 157–162.

[16] Kenning, D. B. R., Konno, T., and Wienecke, M., "Investigation of Boiling Heat Transfer by Liquid Crystal Thermography," *Experimental Thermal and Fluid Science*, Vol. 25, No. 5, 2001, pp. 219–229.

[17] Klausner, J. F., Mei, R., and Chen, W. C., "Liquid Crystal Thermography in Boiling Heat Transfer," *Proceedings of the Society of Photo-Optical Instrumentation Engineers*, International Society for Optical Engineering, Vol. 2546, Bellingham, WA, 1995, pp. 152–159.

[18] Chin, Y., "An Experimental Study on Flow Boiling in a Narrow Channel: From Convective to Nucleate Boiling," Ph.D. Dissertation, Univ. of Houston, Houston, TX, 1997.

[19] Chin, Y., Lakshminarasimhan, M. S., Lu, Q., Hollingsworth, D. K., and Witte, L. C., "Convective Heat Transfer in Vertical Asymmetrically Heated Narrow Channels," *Journal of Heat Transfer*, Vol. 124, No. 6, 2002, pp. 1019–1025.

[20] Aligoodarz, M. R., Yan, Y., and Kenning, D. B. R., "Wall Temperature and Pressure Variation During Flow Boiling in Narrow Channels," *Heat Transfer 1998: Proceedings of the Eleventh International Heat Transfer Conference*, Vol. 2, Korean Society of Mechanical Engineers, Seoul, Korea, distributed by Taylor and Francis, Levittown, PA, 1998, pp. 225–230.

[21] Azar, K., Benson, J. R., and Manno, V. P., "Liquid Crystal Imaging for Temperature Measurement of Electronic Devices," *Proceedings of the Seventh IEEE Semi-Therm Symposium*, Institute of Electrical and Electronics Engineers, Los Alamitos, CA, 1991, pp. 23–33.

[22] Lelea, D., Nishio, S., and Takano, K., "The Experimental Research on Microtube Heat Transfer and Fluid Flow of Distilled Water," *International Journal of Heat and Mass Transfer*, Vol. 47, Nos. 12–13, 2004, pp. 2817–2830.

[23] Owhaib, W., and Palm, B., "Experimental Investigation of Single-Phase Convective Heat Transfer in Circular Microchannnels," *Experimental Thermal and Fluid Science*, Vol. 28, Nos. 2–3, 2004, pp. 105–110.

[24] Hapke, I., Boye, H., and Schmidt, J., "Onset of Nucleate Boiling in Minichannels," *International Journal of Thermal Sciences*, Vol. 39, No. 4, 2000, pp. 505–513.

[25] Fujisawa, N., Aoyama, A., and Kosaka, S., "Measurement of Shear-Stress Distribution Over a Surface by Liquid-Crystal Coating," *Measurement Science and Technology*, Vol. 14, No. 9, 2003, pp. 1655–1661.

[26] Reda, D. C., Muratore, J. J., and Heineck, J. T., "Time and Flow-Direction Responses of Shear-Stress-Liquid Crystal Coatings," *AIAA Journal*, Vol. 32, No. 4, 1994, pp. 693–699.

[27] Hay, H. L., and Hollingsworth, D. K., "A Comparison of Trichromic Systems for Use in the Calibration of Polymer-Dispersed Thermochromic Liquid Crystals," *Experimental Thermal and Fluid Science*, Vol. 12, No. 1, Jan. 1996, pp. 1–12.

[28] Anderson, M., "Thermochromic Liquid Crystal Thermography: Hysterisis, Illumination and Imaging System Effects, Image Processing and Applications," Ph. D. Dissertation, Univ. of California, Davis, Mechanical and Aeronautical Engineering Department, Davis, CA, 1999.

[29] Chan, T. L., Ashforth-Frost, S., and Jambunathan, K., "Calibrating for Viewing Angle Effect During Heat Transfer Measurements on a Curved Surface," *International Journal of Heat and Mass Transfer*, Vol. 44, No. 12, 2001, pp. 2209–2223.

[30] Streeter, V. L., *Handbook of Fluid Dynamics*, 1st ed., McGraw–Hill, New York, 1961, pp. 3-8–3-22.

[31] Kays, W. M., and Crawford, M. E., *Convective Heat and Mass Transfer*, 3rd ed., McGraw–Hill, New York, 1993, pp. 311–354.

[32] Fluorinert, M., "Electronic Liquid FC-72" 3M product information, Maplewood, MN, 2000.

[33] Holman, J. P., *Heat Transfer*, 8th ed., McGraw–Hill, New York, 1997.

[34] Shah, R. K., and London, A. L., "Laminar Flow Forced Convection in Ducts," *In Advances in Heat Transfer*, Academic Press, New York, 1978.

[35] Ebadian, M. A., and Dong, Z. F., "Forced Convection Internal Flow in Ducts," *Handbook of Heat Transfer*, McGraw–Hill, New York, 1998, pp. 5.1–5.32.

[36] Gnielinski, V., "New Equations for Heat and Mass Transfer in Turbulent Pipe and Channel Flow," *International Chemical Engineering*, Vol. 16, No. 2, 1976, pp. 359–368.

[37] Adams, T. S., Abdel-Khalik, S. I., Jeter, S. M., and Qureshi, Z. H., "An Experimental Investigation of Single-Phase Forced Convection in Microchannels," *International Journal of Heat and Mass Transfer*, Vol. 41, Nos. 6–7, 1998, pp. 851–857.